

ARTICLE

Received 19 Sep 2014 | Accepted 5 Jan 2015 | Published 11 Feb 2015

DOI: 10.1038/ncomms7206

OPEN

Control of cytoplasmic dynein force production and processivity by its C-terminal domain

Matthew P. Nicholas^{1,*}, Peter Höök^{2,*†}, Sibylle Brenner¹, Caitlin L. Wynne², Richard B. Vallee^{2,¶} & Arne Gennerich^{1,¶}

Cytoplasmic dynein is a microtubule motor involved in cargo transport, nuclear migration and cell division. Despite structural conservation of the dynein motor domain from yeast to higher eukaryotes, the extensively studied *S. cerevisiae* dynein behaves distinctly from mammalian dyneins, which produce far less force and travel over shorter distances. However, isolated reports of yeast-like force production by mammalian dynein have called interspecies differences into question. We report that functional differences between yeast and mammalian dynein are real and attributable to a C-terminal motor element absent in yeast, which resembles a 'cap' over the central pore of the mammalian dynein motor domain. Removal of this cap increases the force generation of rat dynein from 1 pN to a yeast-like 6 pN and greatly increases its travel distance. Our findings identify the CT-cap as a novel regulator of dynein function.

¹Department of Anatomy and Structural Biology and Gruss-Lipper Biophotonics Center, Albert Einstein College of Medicine, Bronx, New York 10461, USA.

²Department of Pathology and Cell Biology, Columbia University College of Physicians and Surgeons, New York, New York 10032, USA. * These authors contributed equally to this work. ¶ These authors jointly supervised this work. † Present address: Department of Applied and Computational Mathematics and Statistics, University of Notre Dame, 138 Hayes-Healy Center, Notre Dame, Indiana 46556, USA. Correspondence and requests for materials should be addressed to R.B.V. (email: rv2025@cumc.columbia.edu) or to A.G. (email: arne.gennerich@einstein.yu.edu).

Mammalian cytoplasmic dynein plays essential roles in a wide range of both low- and high-force requiring functions during cell division, nuclear positioning and the transport of organelles and mRNAs^{1,2}. In contrast, yeast cytoplasmic dynein is involved in a single, nonessential function, nuclear positioning¹. Interestingly, single-molecule characterization of dynein motor behaviour across species has yielded surprisingly disparate results given the high degree of sequence and structural conservation: whereas purified native mammalian dyneins exhibit a stall force of 1–2 piconewton (pN) (refs 3–5), the extensively studied dimeric *S. cerevisiae* dynein motor domains (MDs) stall at 5–7 pN (refs 6,7). In addition, in the absence of an opposing force, mammalian dyneins move substantially faster than yeast dynein (500 up to >1,000 nm s⁻¹ versus ~100 nm s⁻¹, respectively)^{4,5,7–12} and, under opposing force, maintain attachment to microtubules much less tenaciously (milliseconds to seconds versus tens of seconds, respectively)^{4,6}. The basis for these striking functional differences is unknown.

Dynein is a homodimer of two identical heavy chains, each consisting of a 350–400 kDa ring-shaped MD, a slender ‘tail’ for dimerization and binding of non-catalytic subunits and accessory proteins, and a coiled-coil ‘stalk’ with an MT-binding domain (MTBD)^{1,2}. Each dynein ring consists of six AAA + subunits (AAA: ATPase associated with diverse cellular activities), four of which can bind and/or hydrolyse nucleotide^{13–16}. Mechanochemical analysis has focused on dynein from *S. cerevisiae*, *Dictyostelium discoideum* and mammals. Whereas yeast and *Dictyostelium* studies have predominantly employed recombinant constructs^{6–8,11,13,14,17,18}, mammalian data were until recently^{19–22} mostly from native dynein purified from the brain^{3–5,12,23,24} or cultured cells^{22,25}. Intriguingly, native dynein purified from yeast and artificially dimerized yeast dynein MDs each exhibit much larger stall forces (5–7 pN versus ~1 pN)^{3–7,22} and greater processivity than dyneins from other species (~1–3 μm with runs up to ~20 μm for yeast dynein versus 300–700 nm with runs very rarely exceeding a few micrometres for mammalian dynein)^{4,5,7–11,26}, though substantially slower velocity (~100 nm s⁻¹ for yeast versus 500 up to >1,000 nm s⁻¹ for mammalian dynein)^{4,5,7–12}. These differences may reflect the range of roles for higher eukaryotic dyneins versus the limited physiological function for dynein in *S. cerevisiae*, which serves only to move the nucleus into the bud neck during mitosis¹. However, isolated reports of yeast-like force production by porcine dynein^{23,27} have highlighted the need to better understand dynein force-generating behaviour. Whether differences in dynein function between yeast and mammals (and possibly among mammals) reflect evolutionary variation, protein preparation, experimental conditions or undefined features of dynein mechanical regulation remains a mystery.

Yeast and mammalian dynein motor domains exhibit a high degree of sequence and structural conservation. The only outstanding difference is the presence of a 32 kDa C-terminal motor element in mammals (also present in *Dictyostelium* and other organisms; Fig. 1a,b). This element lies flat over the dynein ring, partially occluding the central pore, and is attached by a flexible, structurally disordered ~20 amino acid (a.a.) predicted ‘hinge’^{14,28,29} to a short helix (H1) emerging from AAA6 (Fig. 1c). The C-terminal extension, referred to here as the CT-cap, also partially covers AAA1, the principle site of ATP hydrolysis (Fig. 1c and inset of Fig. 1c)¹⁵. Prior work revealed that the CT-cap can be separated from the rat MD by limited proteolysis, an effect inhibited by transition state ATP analogues²⁹. Thus, the CT-cap might be structurally independent and capable of shifting position during the mechanochemical cycle²⁹. In *Dictyostelium*, removal of the CT-cap or decreasing the flexibility of the hinge have each been

reported to decrease processivity¹¹. Removal of the entire C-terminal region (CT-cap plus H1) disrupted allosteric communication between the MD and MT-binding domains¹⁴. With this knowledge, we hypothesized that the CT-cap might be responsible for some of the functional differences between yeast and mammalian cytoplasmic dynein.

In this study, we report the first structure-function and single-molecule force measurements of a recombinant dimeric rat dynein motor domain construct. We find that functional differences between yeast and mammalian dynein are real and attributable to a C-terminal motor element absent in yeast, which, when present, resembles a ‘cap’ over the central pore of the dynein motor domain. Removal of this element increases force generation of rat dynein from 1 pN to a yeast-like 6 pN and greatly increases travel distance. Our findings identify the CT-cap as the first motor protein element responsible for controlling force production. The CT-cap potentially represents a novel locus for dynein regulation.

Results

Expression of motor domains with and without the CT-cap.

To test our hypothesis, we generated recombinant, baculovirus-expressed dynein MDs from rat. We engineered two glutathione-S-transferase (GST) fusion constructs (Fig. 1a,b): one corresponding to the wild-type rat dynein (MD-WT) and the other lacking the C-terminal region (MD-ΔCT) and corresponding to *S. cerevisiae* dynein (Fig. 1b). Both constructs omit the dynein tail, but retain the ‘neck’ domain that connects the MD and tail and interacts with the AAA ring in a nucleotide-dependent manner³⁰. Although the tail regulates motor activity^{5,10}, it is nonessential for production of motion and force^{6–8,11,17–19}.

We purified MD-WT and MD-ΔCT using glutathione affinity chromatography (Fig. 1e) (followed by size-exclusion chromatography (SEC) for some preparations; Supplementary Fig. 1a). Each construct ran as a single coherent peak by sucrose density gradient centrifugation with no evidence of aggregation (Supplementary Fig. 1a), and exhibited basal and MT-stimulated ATP hydrolysis (Supplementary Fig. 2 and Supplementary Table 1).

MD-WT motility and force generation. Coverslips coated with MD-WT supported robust MT gliding at up to ~460 nm s⁻¹ (Supplementary Movie 1 and Supplementary Fig. 3), demonstrating clear multi-motor motility. To study MD-WT single-molecule function, we used optical tweezers (Fig. 2a) as described previously³¹. Analysis of the fraction of motile beads as a function of motor concentration (Fig. 2b) showed that single MD-WT particles move and produce forces ≥0.5 pN (~50 nm displacement for a trap stiffness of $k \approx 0.01$ pN nm⁻¹).

At single-molecule concentrations (≤50% beads exhibiting motion), MD-WT exhibited a range of motile behaviour (Fig. 2c and Supplementary Fig. 4). The motor often detached after several steps, and sometimes stalled, with most runs lasting ≤2–3 s and with velocities often exceeding 200 nm s⁻¹. Similar to criteria used previously⁵, we defined stalling as the maximum force achieved and sustained for at least 200 ms during a single-MT encounter (26% of motile events). The MD-WT distribution of stall-forces showed a single peak at 0.9 ± 0.5 pN (mean ± s.d.) (Fig. 2d). Maximal forces (irrespective of duration) were similar, but the distribution was skewed slightly towards smaller forces (Supplementary Fig. 5), indicative of premature MT detachments before stalling⁵ (average run length ~90 ± 50 nm for $k \approx 0.01$ pN nm⁻¹). Prolonged stalling of ≥0.5 s was rare (~9% of events).

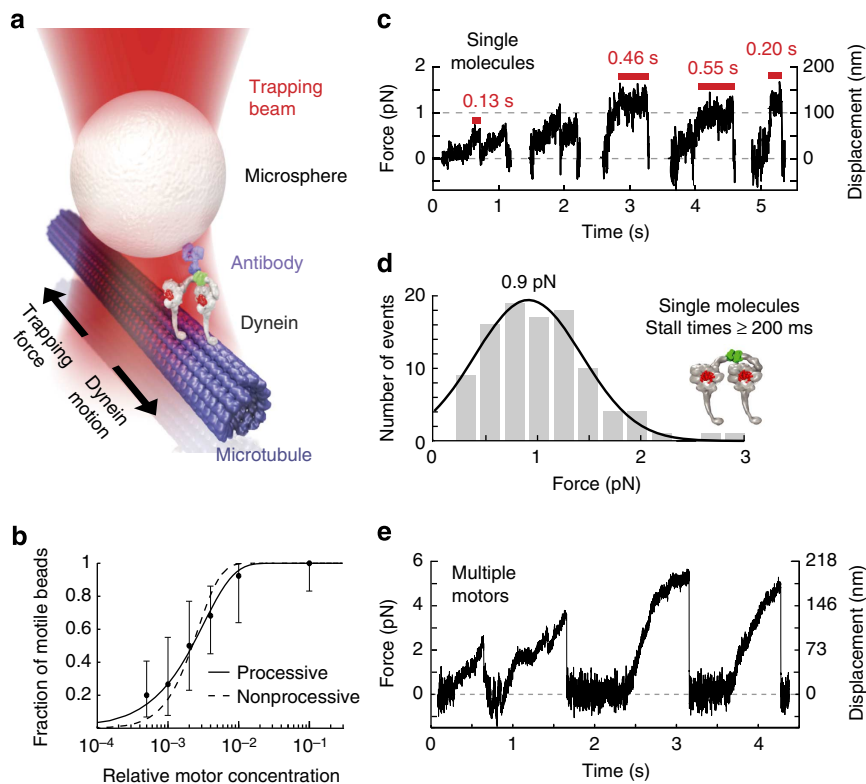


Figure 2 | Single-molecule function of MD-WT. (a) Illustration of the optical trapping assay. GST-dynein is attached via an anti-GST antibody to a 1- μm polystyrene microsphere ('bead') that is optically trapped above a MT. As dynein moves along the MT, the trap exerts an opposing force. (b) Fraction of motile beads (those generating forces ≥ 0.5 pN using a trap stiffness of $k = 0.01$ pN nm $^{-1}$) versus the relative MD-WT concentration. Error bars are Clopper-Pearson 95% confidence intervals (95% CIs) of the mean. We tested 14–25 beads at each concentration (109 total). The curves are fits assuming processive (solid line) or nonprocessive (dashed line) motors (see Methods). The data are best fit by the processive model (coefficient of determination $R^2 = 0.99$ versus $R^2 = 0.91$; F -test P -value = 0.02). (c) Representative examples of MD-WT force generation (1 mM ATP) at motor concentrations for which 50% or fewer beads moved. Red bars indicate duration of maximal sustained force. (d) Histogram of stall forces (maximal forces sustained for ≥ 200 ms), with average 1.0 ± 0.5 pN (mean \pm s.d.). The curve is a Gaussian fit to the data (mean 0.9 pN and s.d. 0.5 pN; 95% CIs (0.8, 1.0) and (0.4, 0.6) pN, respectively). Of 381 MT encounters (derived from 54 beads over 19 experiments), 100 (26%) met the criterion for stalling. (e) Example of large forces produced by MD-WT at high motor concentration (100% fraction of motile beads). Experiments were performed with AC-purified protein (e), with AC-/SEC-purified protein (b,c), and with both AC-purified and AC-/SEC-purified protein (d).

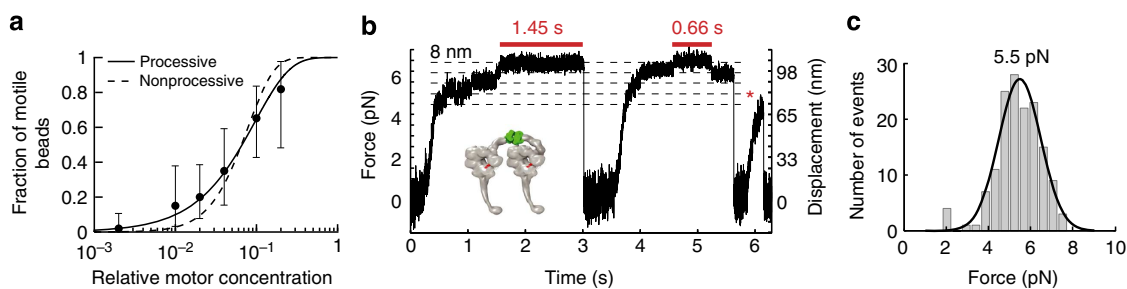


Figure 3 | Force generation of single MD- Δ CT molecules. (a) Processivity analysis, as in Fig. 2b. The data are best fit by the processive model ($R^2 = 0.99$ versus $R^2 = 0.89$; F -test P -value = 0.01). We tested 11–50 beads at each concentration (154 total). (b) Example of single-motor force generation ($k = 0.061$ pN nm $^{-1}$). Steps are visible after reaching ~ 4 pN. The two red bars indicate periods of stalling (here at ~ 6.5 pN). The red asterisk marks a run terminated by detachment before stalling. (c) Histogram of stall forces (maximal forces sustained for ≥ 400 ms), with average 5.4 ± 1.1 pN (mean \pm s.d.) and Gaussian fit (mean 5.5 pN; s.d. 1.0 pN; 95% CIs (5.3, 5.7) and (0.8, 1.2) pN, respectively). Of 340 total MT encounters (derived from 25 beads over 8 separate experiments), 135 (44%) met the stalling criterion. ATP concentration was 1 mM. Experiments were performed with AC-purified protein (a,b) and with both AC-purified and AC-/SEC-purified protein (c).

It tenaciously stalled at 5.5 ± 1.0 pN (mean \pm s.d.) (Fig. 3c), comparable to the behaviour of the analogous yeast dynein construct^{6,7}. To study the MD- Δ CT construct under a constant applied load, we used feedback-based force-clamp experiments in which the optical trap follows bead motion at a fixed distance.

MD- Δ CT routinely moved over 400–500 nm (Fig. 4a), even under loads approaching its stall force (in contrast to MD-WT, for which similar experiments were not feasible due to short run lengths). Velocity-versus-force analysis (Fig. 4b) predicted stalling at 5.7 pN (95% CI (5.1, 6.5) pN), in agreement with our initial

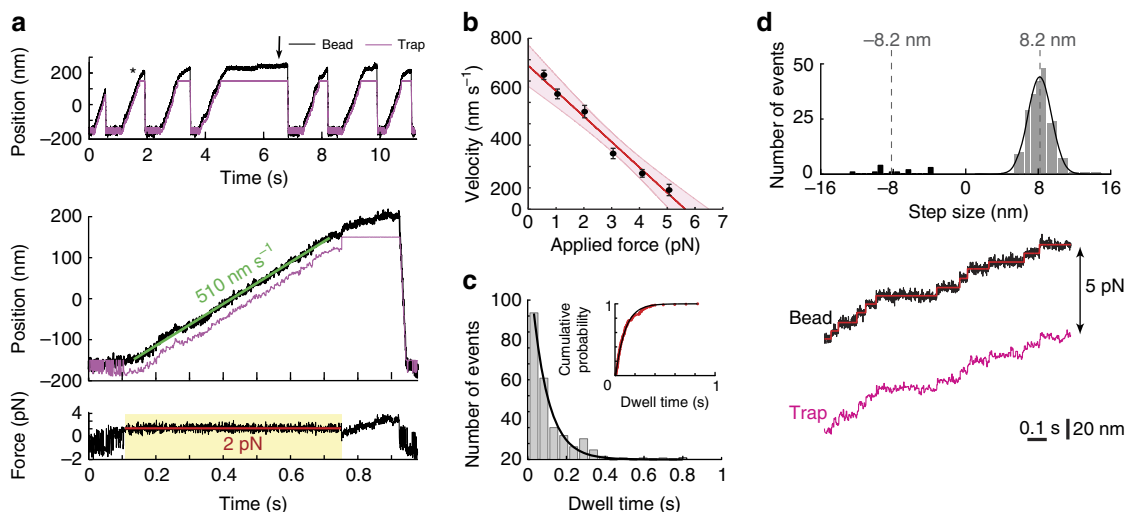


Figure 4 | Single-molecule function of MD- Δ CT. (a) Bead movement under constant load (optical trap force clamp). Top: repeated bead displacements by single motors (black). The trap (magenta) follows at a fixed distance to apply a constant force (here, 2 pN). When the bead travels beyond the region of force-clamp operation, it either stalls (black arrow) or detaches. Bottom: detail of the event marked by an asterisk in the top panel, fit with a line to measure the mean velocity ($\sim 510 \text{ nm s}^{-1}$) during force-clamp operation (yellow region). The lower inset shows the applied force, which was held constant at $2.1 \pm 0.3 \text{ pN}$ (mean \pm s.d.) during force-clamp operation (yellow region). (b) Velocity versus force. Points are means of repeated measurements under constant force, including only runs $\geq 50 \text{ nm}$. Error bars span 95% CIs of the mean. The red line is a weighted linear fit ($V = 672 \text{ nm s}^{-1} - 119 \text{ nm s}^{-1} \text{ pN}^{-1} \times F$), with shaded region of 95% confidence that intercepts the abscissa at (575, 769) nm s^{-1} and the ordinate at (5.1, 6.5) pN. Data are from six beads over two experiments ($N = 38\text{--}233$ at each force; 655 events total). (c) Histogram of dwell times between consecutive forward steps under 5 pN load. An exponential fit, $y = A \exp(-k_{\text{cat}} t)$, gives $k_{\text{cat}} = 12.1 \text{ s}^{-1}$; 95% CI (10.2, 13.9) s^{-1} . Inset: empirical cumulative probability density function, with fit $y = 1 - \exp(-k_{\text{cat}} (t - t_L))$, where t_L is the dwell time detection limit ($\sim 6\text{--}8 \text{ ms}$) and $k_{\text{cat}} = 10.6 \text{ s}^{-1}$ (95% CI (10.4, 10.8) s^{-1}). Data from four beads over three separate experiments (211 events). (d) Top: histogram of step sizes under 5 pN load ($N = 254$). Grey and black bars represent forward (95% of steps) and backward steps, respectively. A Gaussian fit (black curve) to the forward steps yields $8.2 \pm 1.3 \text{ nm}$ (mean \pm s.d.; 95% CI's (8.0, 8.4) and (1.1, 1.5) nm, respectively). Backward steps were $7.8 \pm 2.7 \text{ nm}$ (mean \pm s.d.). Bottom: example trace showing steps (red line) identified by a step-finding algorithm (see Methods). ATP concentration was 1 mM. Experiments were performed with AC-purified protein.

observations (Fig. 3b,c). These findings demonstrate the CT-cap to be a potent regulator of dynein force output and processivity, and suggest that its absence accounts for the greater force generation of yeast dynein.

MD- Δ CT did exhibit some notable differences from the analogous WT yeast dynein constructs. First, MD- Δ CT retains the higher velocity of mammalian dyneins, projected to reach $\sim 670 \text{ nm s}^{-1}$ in the absence of opposing load (intercept with the abscissa in Fig. 4b; Supplementary Fig. 8). Second, MD- Δ CT steps are short and consistent, with few backward steps. Under 5-pN load, the distribution of dwell times between steps is well described by a single exponential (rate constant $k_{\text{cat}} \approx 11\text{--}12 \text{ s}^{-1}$) (Fig. 4c). At this force, MD- Δ CT moves at $\sim 90 \text{ nm s}^{-1}$ (95% CI (64, 117) nm s^{-1}) (Fig. 4b), implying $\sim 8 \text{ nm}$ steps if step size is constant. Direct analysis of step sizes confirms a narrow distribution of $8.2 \pm 1.3 \text{ nm}$ (mean \pm s.d.) with very few (5%) backward steps (Fig. 4d), similar to kinesin³². Resolving steps at low load (0.5 pN force clamp with $5 \mu\text{M}$ ATP) is difficult, but we saw no evidence of increased average step size at low load (Supplementary Fig. 9), in contrast to an earlier study of native mammalian dynein³. The Michaelis–Menten kinetics of velocity observed at 0.5-pN load suggests that step size is also independent of ATP concentration (Supplementary Fig. 8). The stepping behaviour just described differs from that we and others have reported for analogous yeast dynein constructs both in the absence^{8,17,18} and presence⁶ of force. These studies also reported a broader distribution of step sizes, more frequent backward steps, and near the stall force, more 4-nm steps and the emergence of ‘non-advancing’ stepping characterized by repeated forward-backward displacements⁶. Taken together, the differences in velocity and stepping behaviour between yeast

dynein and MD- Δ CT demonstrate that, in addition to the CT-cap, other more subtle variations within the MD may also contribute to interspecies differences between dyneins.

Discussion

Here, using combined structure-function and single-molecule force measurements on a recombinant GST-dimerized rat dynein, we demonstrate that functional differences between yeast and mammalian dynein are primarily attributable to the relatively little explored C-terminal motor domain structure, which is absent in yeast and present in mammalian dynein as a ‘cap’ over the central pore of the motor domain. Removal of the CT-cap imparts rat dynein with increased processivity and yeast dynein-like force-generation capabilities. We speculate that the CT-cap may act as a target for regulatory factors and/or post-translational modifications responsible for modulating mammalian dynein processivity and force output for dynein’s numerous and diverse cellular functions. For example, modification of the CT-cap could help fine-tune dynein’s force generation for high-load functions, such as nucleokinesis, and low-load functions, including the long-distance transport of mRNA and vesicles.

The underlying molecular mechanism by which the CT-cap regulates dynein force production and processivity now emerges as an important question in the field. Intriguingly, the CT-cap lies over the ATPase cleft of AAA1-AAA2 (ref. 14), suggesting a potential role in regulating nucleotide access to dynein’s main active site. Proteolytic removal of the CT-cap is sensitive to nucleotide occupancy of this site, and more immediately significant, ATPase activity is reduced and the K_i for vanadate markedly increased on the removal of the CT-cap²⁹.

Crystallographic analysis revealed residual nucleotide in AAA1 for the *Dictyostelium* MD, but not yeast^{13,14}, consistent with a decrease in affinity for ATP. Thus, the CT-cap may operate as a shutter to open or close the AAA1-AAA2 ATPase cleft, with the effect of destabilizing or stabilizing ATP/ADP binding. Nucleotide may exchange more freely in the absence of the CT-cap, resulting in reduced ATP and/or ADP affinities and prolongation of the apo MT-binding state. Extending or shortening the duration of specific steps in the mechanochemical cycle could affect force-bearing states of the dynein cross-bridge cycle and consequently increase the motor's stall force and processivity. Whether such changes prove valid remains to be tested. In addition, the CT-cap may affect allosteric communication between the AAA ring and MTBD, as shown for a complete C-terminal truncation of the *Dictyostelium* MD (that is, CT-cap plus H1 (ref. 14); see Supplementary Information for an extended discussion).

Our findings reveal that the removal of the CT-cap increases the processivity of dynein. Whereas the MD-WT motor moves on average over ~ 90 nm under loads up to 0.5 pN, MD- Δ CT movement routinely exceeds the 400 nm detection range of our microscope, even under loads of up to 5 pN. These data provide the first evidence that dynein processivity can be controlled by elements within the motor itself. This is in contrast to the finding that a truncation of the *Dictyostelium* dynein C-terminus resulted in a non-processive motor¹¹, perhaps attributable to the use of different termination sites (the *Dictyostelium* truncation site was distal to the one employed here and to the C-terminal boundary in yeast). Dynactin has long been known for its role in increasing dynein processivity by approximately twofold³³, an effect recently shown to be mediated by a dynein binding, coiled-coiled element in the p150^{Glued} subunit of dynactin^{9,34}. Recent work has also demonstrated that the dynactin-cargo adapter protein BicD2 markedly enhances dynein processivity by stabilizing the dynein-dynactin complex, thereby converting mammalian dynein into an ultra processive motor, which moves over distances of up to ~ 10 μ m (refs 20,21). The relationship between such factors, and dynactin- and CT-cap-regulated processivity remains to be addressed in detail.

The enhanced processivity of the MD- Δ CT construct allowed us to determine its force-velocity (F - V) relationship using the force-clamp mode of our optical tweezers. Recent work has shown that the shape of the F - V curve provides insight into the motor's ability to work cooperatively in multi-motor assemblies^{35,36}. We note that the measured F - V curve for the MD- Δ CT construct (Fig. 4b) differs in shape from the F - V curve reported for full-length yeast dynein⁶. While the F - V curve of yeast dynein is sigmoidal, the F - V curve of the MD- Δ CT motor can be approximated by a linear function. Different F - V curves can be expected considering that yeast dynein shows force-dependent stepping behaviour, while MD- Δ CT exhibits a unitary, load-independent step size. However, given the experimental uncertainty of our measurements at low loads (< 2 pN) and high loads (> 4 pN), we are hesitant to conclude which underlying differences between the motors account for the F - V curves.

Interestingly, the MD- Δ CT motor differs in stepping behaviour from that reported for higher eukaryotic full-length dyneins. The ~ 6 pN-generating MD- Δ CT construct displayed a unitary 8-nm step size independent of load, in contrast to the load-dependent stepping behaviour reported for ~ 1 pN-generating mammalian dynein^{3,37}. Because full-length yeast dynein and the GST-dimerized yeast dynein construct analogous to our MD- Δ CT motor have similar stepping behaviours⁶, it is unlikely that the truncation and GST-dimerization of MD- Δ CT account for the difference. The possibility that the CT-cap can alter stepping behaviour, in addition to its impact on force generation and

processivity, requires further investigation. Indeed, while full-length and truncated GST-dimerized yeast motors show load-dependent stepping behaviour, their predominant advancing step size is 8 nm even at low load⁶, as is the case for the MD- Δ CT motor. Thus, it is possible that the presence of the CT-cap in mammalian dynein affects the forward displacement of the trailing head. Presumably, the CT-cap of one motor domain is sandwiched between both motor domains, and could therefore influence the path of the rear head as it moves forward (for example, by sterically affecting head passing and/or linker element movements), biasing the motor towards larger steps under low load.

In conclusion, we have elucidated a novel role for the relatively little explored dynein CT-cap and explain previously puzzling differences between yeast and mammalian dynein. It remains to be seen how this domain exerts its effects. Future studies promise exciting insights into the mechanisms by which the CT-cap regulates the dynein nanomachine.

Methods

Construct design. Two dynein MD fragments, one of 399 kDa (MD-WT; a.a. 1157–4644) encompassing the entire MD and another of 367 kDa (MD- Δ CT; a.a. 1157–4348) lacking the CT-cap, were cloned from the full-length rat cytoplasmic dynein heavy chain and produced by the baculovirus expression system. The MD fragments were N-terminally fused with an in-frame GST tag for rapid purification and MD dimerization. The proper C-terminal boundary of MD- Δ CT was determined from primary sequence alignment and X-ray crystallography structural data of *D. discoideum*^{14,28} and *S. cerevisiae*^{13,38} dynein.

Dynein expression and purification. Sf9 insect cells were infected with recombinant baculovirus for 50–55 h. The cells were washed in PBS, and recombinant dynein was extracted by homogenization in DEB (100 mM Pipes, pH 7.2, 2 mM MgCl₂, 2 mM EGTA, 50 mM NaCl, 1 M glycerol, 0.1 mM ATP, 1 mM DTT, protease inhibitor cocktail (Sigma)). The cytosolic extract was cleared by centrifugation at 5,000 g for 10 min and 100,000 g for 30 min. The supernatant was applied to a GST SpinTrap purification column (GE Healthcare) and incubated for 20 min at 4 °C. Unbound material was removed by washing the column two times with DEB, and bound protein was eluted with 10 mM glutathione in DB (30 mM Pipes, pH 7.2, 2 mM MgCl₂, 2 mM EGTA, 50 mM NaCl, 1 M glycerol, 1 mM DTT). In some preparations, free GST was removed by SEC fractionation on a gravity flow column manually packed with 2 ml Sephacryl S-200 (GE Healthcare) in DB (removal of free GST from MD-WT or MD- Δ CT samples by SEC did not affect the force-generation capabilities of the motor constructs, as judged by the consistent motor behaviour before and after the additional purification step). Protein concentrations, which varied between 0.1–0.2 mg ml⁻¹ depending on the prep, were determined by the Bradford method, using albumin as a standard, and by densitometric analysis of band intensities on a coomassie-stained sodium dodecyl sulfate-PAGE (SDS-PAGE) gel. Purified dynein was assayed for enzymatic activity within 1 day. For single-molecule analyses, small aliquots of protein were immediately distributed to thin-walled PCR tubes, flash-frozen in liquid nitrogen and stored at -80 °C pending use.

Sucrose gradient density ultracentrifugation. For sucrose gradient analysis, purified MD-WT and MD- Δ CT were loaded onto a 1.3-ml linear 5–20% sucrose gradients in DB buffer (30 mM Pipes, pH 7.2, 2 mM MgSO₄, 2 mM EGTA, 50 mM NaCl, 1 M glycerol, 1 mM DTT). The gradients were centrifuged at 54,000 r.p.m. for 3 h at 4 °C in a Beckman TLS-55 rotor. Fractions were collected and analysed by SDS-PAGE and western blot using a monoclonal GST antibody (1E5, Santa Cruz Biotech, 1:1,000).

Optical trapping. Optical trapping studies were performed essentially as described previously in detail^{31,39}. Cy3-labelled MTs were bound covalently to amino-silanated glass coverslips, which were then used to make flow chambers. After appropriate dilution in assay buffer (30 mM PIPES, 2 mM MgSO₄, 2 mM EGTA, 7.3% glycerol, 10 μ M taxol, pH 7.2) with 1 mg ml⁻¹ β -casein, dynein was bound to 1- μ m diameter polystyrene microspheres covalently bound to anti-GST antibodies. The mixture was then supplemented with ATP (1 mM), DTT (10 mM), a pyranose oxidase-based oxygen scavenger system⁴⁰ (25 mM glucose, 3 U ml⁻¹ pyranose oxidase and 90 U ml⁻¹ catalase) and β -casein (1 mg ml⁻¹), and flowed into the slide chamber. In some experiments (including all experiments studying titration of ATP), an ATP regeneration system was also added (1 mM phosphoenolpyruvate, 0.1 mg ml⁻¹ pyruvate kinase). The optical trapping microscope, including the automated force clamp, was controlled using software custom-written in LABVIEW (National Instruments). Data were acquired at 3 kHz after low-pass

filtering at 1.5 kHz. Beads were tested for at least 4 min each to determine the presence of active motors. For analysis of single-molecule behaviour, data were considered only if 50% or fewer beads from the given experiment exhibited motility⁴¹, which was achieved by diluting the purified MD-WT and MD- Δ CT motor constructs 100–500 \times and 10–100 \times , respectively, in the assay buffer. Data visualization and analysis were performed using software custom-written in MATLAB (The MathWorks).

Processivity analysis. We defined beads as motile if they generated ≥ 0.5 pN at least once during a 4 min observation period (generally, $k = 0.01$ pN nm⁻¹ for MD-WT or $k = 0.04$ – 0.06 pN nm⁻¹ for MD- Δ CT, with spring constants chosen such that stalling usually occurred at ~ 100 – 200 nm bead displacement). We then plotted the motile fraction versus relative motor concentration and calculated the uncertainty in each measurement (which constitutes sampling from a binomial population, that is, motile beads and non-motile beads), as the Clopper-Pearson 95% CI of the mean. We fit two models⁴² (weighted by the uncertainty in each measurement) to the data. The first, ‘processive’ model assumes one or more motors are required to move a bead: $F = 1 - \exp(-\lambda C)$, where F is the fraction of moving beads, C is the relative motor concentration and λ is a fitting parameter that depends on the fraction of active motors. The second, ‘nonprocessive’ model assumes two or more motors are required: $F = 1 - \exp(-\lambda C) - (\lambda C) \exp(-\lambda C)$. We determined which model fit best by considering the coefficient of determination (R^2) for each fit and a one-parameter F -test at significance level $\alpha = 0.05$.

Stall force analysis. The stalling criterion for MD-WT was chosen empirically and based on previous work⁵. For MD- Δ CT, which robustly maintains attachment to the MT, and continues to advance slowly as it approaches stall force, we employed a somewhat more systematic approach to ensure that stalling events excluded detachment before reaching the true maximal force. We first picked candidate stalling events of ~ 200 ms or longer. On this data set, we performed a Lilliefors goodness-of-fit test of composite normality at the $\alpha = 0.05$ significance level, under the null hypothesis that the stall forces were normally distributed (with unspecified mean and standard deviation). The test initially rejected the null hypothesis, suggesting a non-normal distribution of data. This is unexpected for true stalling events, and likely indicates that some events represented detachment from the MT before stalling occurred. We then applied a new threshold, picking only events lasting ≥ 250 ms, and repeated the test, again rejecting the null hypothesis. Repeating this procedure again for 300 or 400 ms threshold failed to reject the null hypothesis. We then used 400 ms as our stall-time criterion. The difference in the calculated mean for either case was small (5.3 pN for 200 ms threshold versus 5.5 pN for 400 ms threshold, or a 4% change).

Force-clamp experiments. In custom software that controls our microscope, we implemented a simple force-clamp (force-feedback) algorithm with a proportional gain response to offsets from the force set-point. Depending on the motor velocity, we employed a feedback rate of 50–600 Hz (higher rates are required for greater velocities). During these experiments, we periodically turned off the force feedback and confirmed that the stalling behaviour was unaffected. This was done to rule out damage due to prolonged application of the constant loads. To determine average velocities for velocity versus force and Michaelis–Menten plots, we fit lines to runs ≥ 50 nm in length, and computed the average of all measurements (line fits) and then the 95% CI as $1.96 \times$ s.e.m. Linear and nonlinear curve fitting was performed in MATLAB (The MathWorks) or R (www.R-project.org), and 95% CIs for the parameters were calculated with built-in functions (with Bonferroni correction for simultaneous parameter estimation, where appropriate). For dwell time and step size analysis, the locations and sizes of steps were detected using an automatic detection algorithm⁴³, as described previously⁶.

Basal and microtubule-stimulated ATPase activities. MD-WT and MD- Δ CT were enzymatically tested for steady-state ATPase activity using the Malachite Green assay. Dynein activity was assayed at 25 °C for 30 min in DAB (30 mM Pipes, 2 mM MgCl₂, 2 mM EGTA, 7.3% glycerol, 1 mM DTT, pH 7.2) supplemented with 0–5 mM ATP and in the absence and presence of 0.1–20 μ M taxol-stabilized microtubules (tubulin; Cytoskeleton). Control samples of microtubules alone were included in the analysis. Computed ATPase activities were corrected for the presence of free GST by determining total amount of protein and the fraction of free GST by densitometric analysis of band intensities on a coomassie-stained SDS-PAGE gel.

Microtubule gliding. Coverslips (Zeiss) were cleaned using the HCl-Ethanol protocol from the Salmon lab (<http://labs.bio.unc.edu/Salmon/protocolscoverslippreps.html>). In short, coverslips were submerged in 1 M HCl for 16 h at 60 °C, followed by intensive rinsing with ddH₂O and threefold sonication in ddH₂O for 30 min. Subsequently, the coverslips were sonicated sequentially for 30 min each in ethanol solutions of 50% (V/V), 75% (V/V) and 95% (V/V), respectively. The coverslips were stored in 200-proof ethanol and flamed immediately before use.

MT-gliding assays were performed on a total internal reflection fluorescence (TIRF) microscope (modified Nikon Eclipse Ti) with a $\times 100$, 1.45 NA oil immersion objective (Nikon) and a 532-nm laser (Coherent) to excite TRITC (tetramethyl rhodamine isothiocyanate)-labelled MTs (Cytoskeleton). Images were obtained using μ Manager⁴⁴ and an EMCCD (electron multiplier CCD; Andor iXon Ultra) with an acquisition time of 1,000 ms. The assay buffer consisted of 30 mM PIPES, 2 mM EGTA, 2 mM MgSO₄, 7.3% glycerol, 1 mM DTT, 20 μ M taxol, pH 7.2. Rat brain dynein was attached to the coverslip by non-specific binding; rat GST dynein was linked to the coverslip via an anti-GST antibody (Abcam ab6613, diluted 1 in 10 in dynein buffer and bound non-specifically to the coverslip). Next, the coverslip surface was blocked with 2 mg ml⁻¹ BSA in assay buffer. Finally, the motility solution containing 2 mg ml⁻¹ BSA and varying concentrations of ATP, an ATP-regeneration system (see above), an oxygen scavenger system (see above) and 0.05 mg ml⁻¹ TRITC-MTs was added. Data were analysed using ImageJ^{45,46} (in conjunction with the plugin MTrackJ⁴⁷) and the data analysis software Prism (GraphPad Software).

Dynein-MT co-sedimentation and release. Fifty microlitres of purified dynein (concentration 100 to 350 ng μ l⁻¹, depending on the MD construct) was supplemented with 20 μ M taxol (Cytoskeleton), mixed with 2 to 3 μ M MTs (tubulin; Cytoskeleton) and incubated at 37 °C. The mixture (‘input’) was layered onto 100 μ l of 25% sucrose (containing 20 μ M taxol, and 1 mM DTT) and centrifuged at 60,000 g for 10 min at 25 °C in a TLA120 rotor (Beckman). The remaining supernatant (‘S1’) was discarded and the pellet washed with 50 μ l dynein ‘wash buffer’ (containing 20 μ M taxol and 1 mM DTT), and then resuspended in wash buffer with 5 mM ATP (‘P1’). The solution was centrifuged again using the same parameters as above, the supernatant (‘S2’) was reserved and the pellet (‘P2’) was discarded. During the procedure, 5 μ l each of input, S1, P1, S2 and P2 were reserved for SDS-PAGE analysis, as in Supplementary Fig. 7.

Three-dimensional model rendering and figure preparation. Figures 1c,d and 2a were created with VMD⁴⁸ and The Persistence of Vision Raytracer (POV-Ray, <http://www.povray.org/>) using PDB entries 3VKH, 3J2U, 1VF4 and 1IGT.

References

- Kardon, J. & Vale, R. Regulators of the cytoplasmic dynein motor. *Nat. Rev. Mol. Cell Biol.* **10**, 854–865 (2009).
- Vallee, R. B., McKenney, R. J. & Ori-McKenney, K. M. Multiple modes of cytoplasmic dynein regulation. *Nat. Cell Biol.* **14**, 224–230 (2012).
- Mallik, R., Carter, B. C., Lex, S. A., King, S. J. & Gross, S. P. Cytoplasmic dynein functions as a gear in response to load. *Nature* **427**, 649–652 (2004).
- McKenney, R. J., Vershinin, M., Kunwar, A., Vallee, R. B. & Gross, S. P. LIS1 and NudE induce a persistent dynein force-producing state. *Cell* **141**, 304–314 (2010).
- Ori-McKenney, K. M., Xu, J., Gross, S. P. & Vallee, R. B. A cytoplasmic dynein tail mutation impairs motor processivity. *Nat. Cell Biol.* **12**, 1228–1234 (2010).
- Gennerich, A., Carter, A. P., Reck-Peterson, S. L. & Vale, R. D. Force-induced bidirectional stepping of cytoplasmic dynein. *Cell* **131**, 952–965 (2007).
- Cho, C., Reck-Peterson, S. L. & Vale, R. D. Regulatory ATPase sites of cytoplasmic dynein affect processivity and force generation. *J. Biol. Chem.* **283**, 25839–25845 (2008).
- Reck-Peterson, S. L. *et al.* Single-molecule analysis of dynein processivity and stepping behavior. *Cell* **126**, 335–348 (2006).
- Kardon, J. R., Reck-Peterson, S. L. & Vale, R. D. Regulation of the processivity and intracellular localization of *Saccharomyces cerevisiae* dynein by dynactin. *Proc. Natl Acad. Sci. USA* **106**, 5669–5674 (2009).
- Rao, L. *et al.* The yeast dynein Dyn2-Pac11 complex is a dynein dimerization/processivity factor: structural and single-molecule characterization. *Mol. Biol. Cell* **24**, 2362–2377 (2013).
- Numata, N., Shima, T., Ohkura, R., Kon, T. & Sutoh, K. C-sequence of the Dictyostelium cytoplasmic dynein participates in processivity modulation. *FEBS Lett.* **585**, 1185–1190 (2011).
- Paschal, B. M., Shpetner, H. S. & Vallee, R. B. MAP 1C is a microtubule-activated ATPase which translocates microtubules in vitro and has dynein-like properties. *J. Cell Biol.* **105**, 1273–1282 (1987).
- Schmidt, H., Gleave, E. S. & Carter, A. P. Insights into dynein motor domain function from a 3.3-Å crystal structure. *Nat. Struct. Mol. Biol.* **19**, 492–497 (2012).
- Kon, T. *et al.* The 2.8 Å crystal structure of the dynein motor domain. *Nature* **484**, 345–350 (2012).
- Gibbons, I. R., Gibbons, B. H., Mocz, G. & Asai, D. J. Multiple nucleotide-binding sites in the sequence of dynein beta heavy chain. *Nature* **352**, 640–643 (1991).
- Kon, T., Nishiura, M., Ohkura, R., Toyoshima, Y. Y. & Sutoh, K. Distinct functions of nucleotide-binding/hydrolysis sites in the four AAA modules of cytoplasmic dynein. *Biochemistry* **43**, 11266–11274 (2004).
- Qiu, W. *et al.* Dynein achieves processive motion using both stochastic and coordinated stepping. *Nat. Struct. Mol. Biol.* **19**, 193–200 (2012).

18. DeWitt, M. A., Chang, A. Y., Combs, P. A. & Yildiz, A. Cytoplasmic dynein moves through uncoordinated stepping of the AAA + ring domains. *Science* **335**, 221–225 (2012).
19. Trokter, M., Mücke, N. & Surrey, T. Reconstitution of the human cytoplasmic dynein complex. *Proc. Natl Acad. Sci. USA* **109**, 20895–20900 (2012).
20. McKenney, R. J., Huynh, W., Tanenbaum, M. E., Bhabha, G. & Vale, R. D. Activation of cytoplasmic dynein motility by dynactin-cargo adapter complexes. *Science* **345**, 337–341 (2014).
21. Schlager, M. A., Hoang, H. T., Urnavicius, L., Bullock, S. L. & Carter, A. P. In vitro reconstitution of a highly processive recombinant human dynein complex. *EMBO J.* **33**, 1855–1868 (2014).
22. Torisawa, T. *et al.* Autoinhibition and cooperative activation mechanisms of cytoplasmic dynein. *Nat. Cell Biol.* **16**, 1118–1124 (2014).
23. Toba, S., Watanabe, T. M., Yamaguchi-Okimoto, L., Toyoshima, Y. Y. & Higuchi, H. Overlapping hand-over-hand mechanism of single molecular motility of cytoplasmic dynein. *Proc. Natl Acad. Sci. USA* **103**, 5741–5745 (2006).
24. Walter, W. J., Brenner, B. & Steffen, W. Cytoplasmic dynein is not a conventional processive motor. *J. Struct. Biol.* **170**, 266–269 (2010).
25. Kobayashi, T. & Murayama, T. Cell cycle-dependent microtubule-based dynamic transport of cytoplasmic dynein in mammalian cells. *PLoS ONE* **4**, e7827 (2009).
26. Mallik, R., Petrov, D., Lex, S. A., King, S. J. & Gross, S. P. Building complexity: an in vitro study of cytoplasmic dynein with in vivo implications. *Curr. Biol.* **15**, 2075–2085 (2005).
27. Walter, W. J., Koonce, M. P., Brenner, B. & Steffen, W. Two independent switches regulate cytoplasmic dynein's processivity and directionality. *Proc. Natl Acad. Sci. USA* **109**, 5289–5293 (2012).
28. Kon, T., Sutoh, K. & Kurisu, G. X-ray structure of a functional full-length dynein motor domain. *Nat. Struct. Mol. Biol.* **18**, 638–642 (2011).
29. Höök, P. *et al.* Long range allosteric control of cytoplasmic dynein ATPase activity by the stalk and C-terminal domains. *J. Biol. Chem.* **280**, 33045–33054 (2005).
30. Roberts, A. J. *et al.* ATP-driven remodeling of the linker domain in the dynein motor. *Structure* **20**, 1670–1680 (2012).
31. Nicholas, M. P., Rao, L. & Gennerich, A. An improved optical tweezers assay for measuring the force generation of single kinesin molecules. *Methods Mol. Biol.* **1136**, 171–246 (2014).
32. Svoboda, K., Schmidt, C. F., Schnapp, B. J. & Block, S. M. Direct observation of kinesin stepping by optical trapping interferometry. *Nature* **365**, 721–727 (1993).
33. King, S. J. & Schroer, T. A. Dynactin increases the processivity of the cytoplasmic dynein. *Nat. Cell Biol.* **2**, 20–24 (2000).
34. Tripathy, S. K. *et al.* Autoregulatory mechanism for dynactin control of processive and diffusive dynein transport. *Nat. Cell Biol.* **16**, 1192–1201 (2014).
35. Driver, J. W. *et al.* Productive cooperation among processive motors depends inversely on their mechanochemical efficiency. *Biophys. J.* **101**, 386–395 (2011).
36. Jamison, D. K., Driver, J. W., Rogers, A. R., Constantinou, P. E. & Diehl, M. R. Two kinesins transport cargo primarily via the action of one motor: implications for intracellular transport. *Biophys. J.* **99**, 2967–2977 (2010).
37. Rai, A. K., Rai, A., Ramaiya, A. J., Jha, R. & Mallik, R. Molecular adaptations allow dynein to generate large collective forces inside cells. *Cell* **152**, 172–182 (2013).
38. Carter, A. P., Cho, C., Jin, L. & Vale, R. D. Crystal structure of the dynein motor domain. *Science* **331**, 1159–1165 (2011).
39. Nicholas, M. P., Rao, L. & Gennerich, A. Covalent immobilization of microtubules on glass surfaces for molecular motor force measurements and other single-molecule assays. *Methods Mol. Biol.* **1136**, 137–169 (2014).
40. Svoboda, M. *et al.* Enzymatic oxygen scavenging for photostability without pH drop in single-molecule experiments. *ACS Nano* **24**, 6364–6369 (2012).
41. Gutiérrez-Medina, B., Fehr, A. N. & Block, S. M. Direct measurements of kinesin torsional properties reveal flexible domains and occasional stalk reversals during stepping. *Proc. Natl Acad. Sci. USA* **106**, 17007–17012 (2009).
42. Svoboda, K. & Block, S. M. Force and velocity measured for single kinesin molecules. *Cell* **77**, 773–784 (1994).
43. Kerssemakers, J. W. J. *et al.* Assembly dynamics of microtubules at molecular resolution. *Nature* **442**, 709–712 (2006).
44. Edelstein, A., Amodaj, N., Hoover, K., Vale, R. & Stuurman, N. Computer control of microscopes using μ Manager. *Curr. Protoc. Mol. Biol.* **92**, 14.20.1–14.20.17 (2010).
45. Abramoff, M. D., Magalhães, P. J. & Ram, S. J. Image processing with ImageJ. *Biophoton. Int.* **11**, 36–42 (2004).
46. Schneider, C. A., Rasband, W. S. & Eliceiri, K. W. NIH Image to ImageJ: 25 years of image analysis. *Nat. Method* **9**, 671–675 (2012).
47. Meijering, E., Dzyubachyk, O., Smal, I. & van Cappellen, W. A. Tracking in cell and developmental biology. *Semin. Cell Dev. Biol.* **20**, 894–902 (2009).
48. Humphrey, W., Dalke, A. & Schulten, K. VMD: visual molecular dynamics. *J. Mol. Graph.* **14**, 33–38 (1996).

Acknowledgements

This work was supported by grants GM094415 (A.G.), GM102347 (R.B.V) and T32GM007288 (M.P.N.) from the US National Institutes of Health, a research development grant from the Muscular Dystrophy Association (P.H.) and a German Research Foundation (DFG) postdoctoral grant BR 4257/1-1 (S.B.). We thank Sarah Weil for providing purified native rat dynein. M.P.N. thanks Laura Nicholas and Edward Manning for assistance with figure preparation.

Author contributions

P.H. and R.V. conceived the project. P.H. designed and engineered recombinant MD-WT and MD- Δ ACT motor constructs, performed solution-based kinetic analysis, and with C.G.L. produced the protein. M.P.N. and A.G. designed and performed the optical trapping experiments and analyses. A.G. performed dynein-MT co-sedimentation experiments. S.B. designed and performed the MT-gliding experiments and optimized the dynein-MT co-sedimentation assay. M.P.N., S.B., P.H., R.B.V. and A.G. wrote the paper.

Additional information

Supplementary Information accompanies this paper at <http://www.nature.com/naturecommunications>

Competing financial interests: The authors declare no competing financial interests.

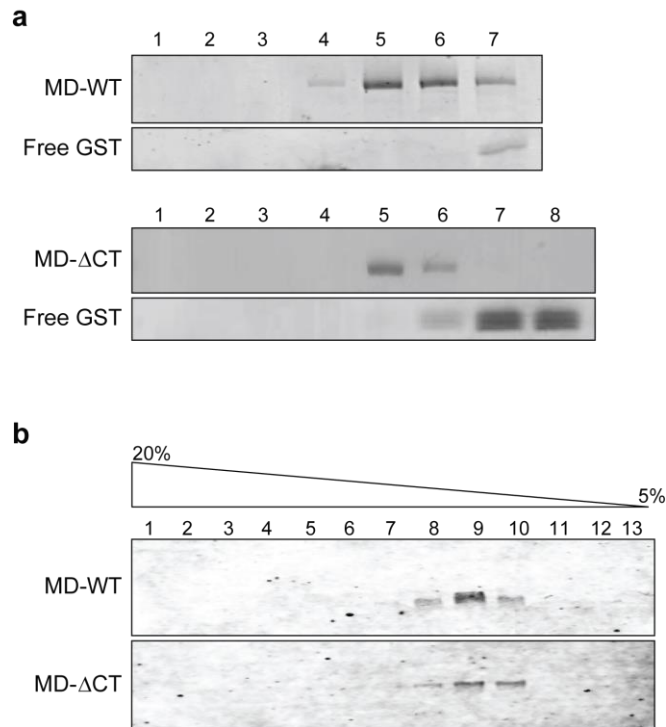
Reprints and permission information is available online at <http://npg.nature.com/reprintsandpermissions/>

How to cite this article: Nicholas M. P. *et al.* Control of cytoplasmic dynein force production and processivity by its C-terminal domain. *Nat. Commun.* **6**:6206 doi: 10.1038/ncomms7206 (2015).

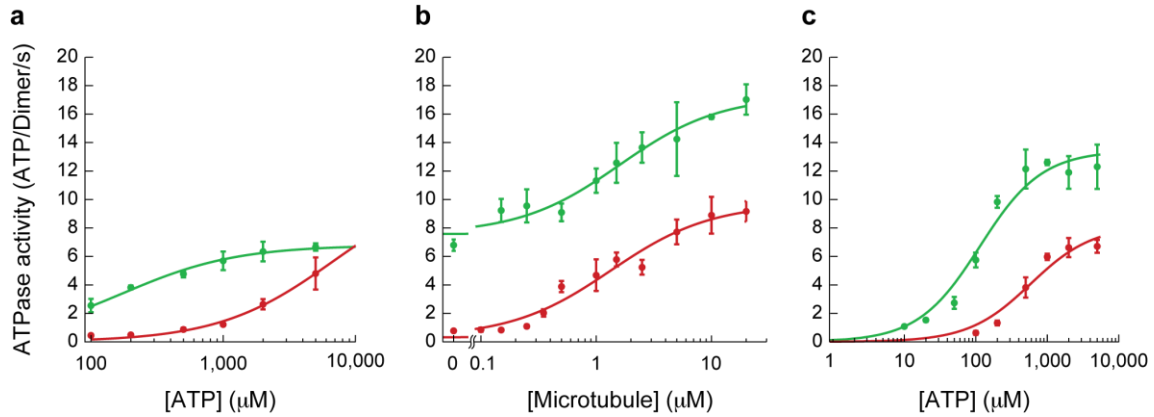


This work is licensed under a Creative Commons Attribution 4.0 International License. The images or other third party material in this article are included in the article's Creative Commons license, unless indicated otherwise in the credit line; if the material is not included under the Creative Commons license, users will need to obtain permission from the license holder to reproduce the material. To view a copy of this license, visit <http://creativecommons.org/licenses/by/4.0/>

Supplementary Figures:

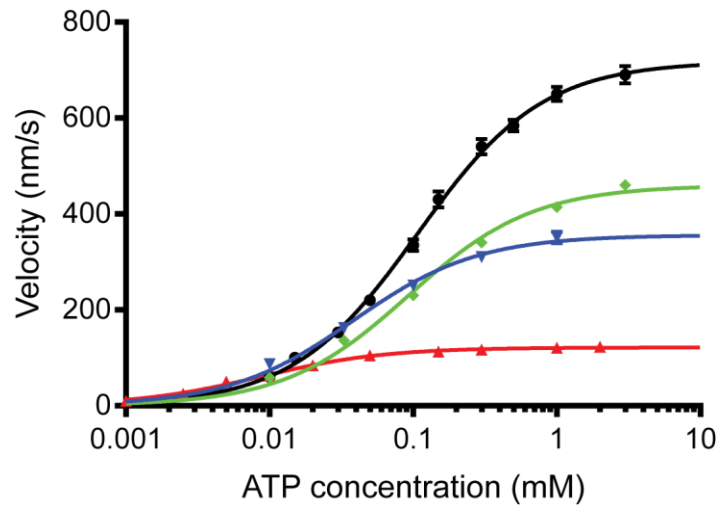


Supplementary Figure 1 | Size-exclusion chromatography purification and sucrose density gradient centrifugation. (a) Representative SDS-PAGE gels of size-exclusion chromatography fractionated MD-WT and MD- Δ CT preparations. Complete separation of free GST from MD-WT (fraction 5 and 6) and MD- Δ CT (fraction 5) were achieved. No evidence of larger aggregates was observed in the void volume (fraction 3). (b) Western blot analysis using anti-GST antibodies of the purified MD-WT and MD- Δ CT dynein after sucrose density gradient centrifugation and fractionation. Each preparation shows a single symmetric peak, indicative of a monodisperse dynein species. Faster sedimenting protein aggregates were not observed, nor was aggregated protein detected in sample from bottom of the centrifuge (fraction 1). Also, we saw no evidence for contaminating regulatory factors by Coomassie Blue staining, nor did we detect any Lis1 contamination by immunoblotting.

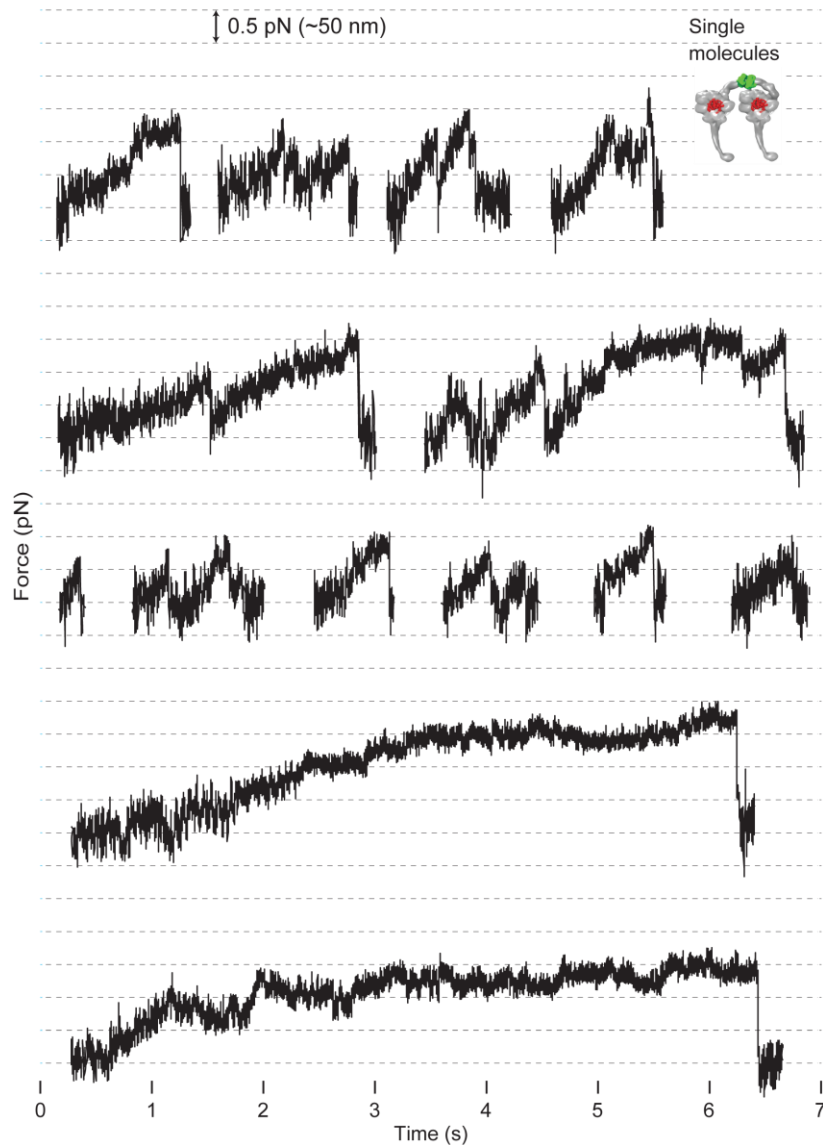


Supplementary Figure 2 | ATPase activity of MD-WT (green) and MD- Δ CT (red). (a)

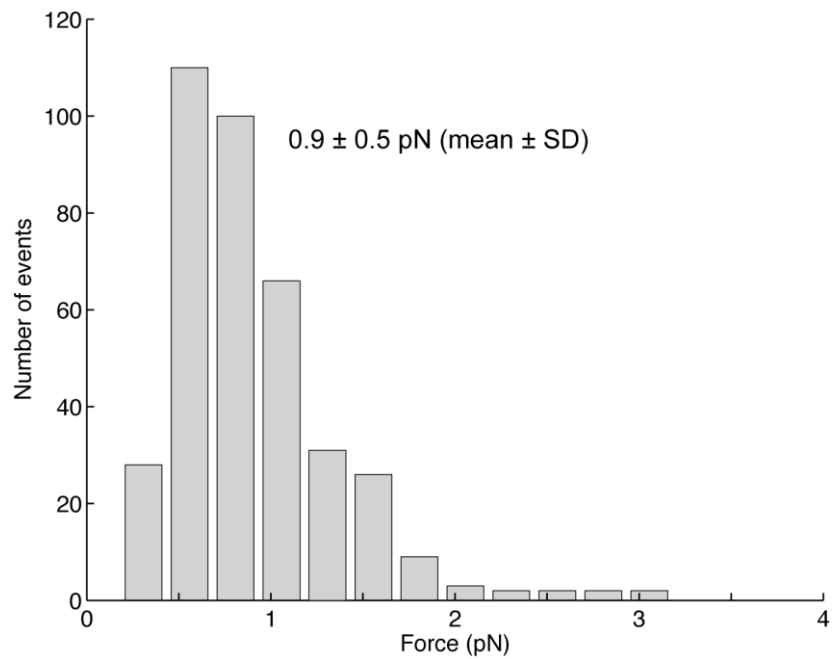
ATPase activity as a function of ATP concentration in the absence of MTs. The lines are fits using the Michaelis-Menten equation, $k_{\text{obs}} = k_{\text{cat}} \times [\text{ATP}] / (K_M(\text{ATP}) + [\text{ATP}])$. **(b)** ATPase activity as a function of MT concentration, in the presence of 1 mM ATP. The lines are fits using the equation (3) $k_{\text{obs}} = (k_{\text{cat}} - k_{\text{basal}}) \times [\text{MT}] / (K_M(\text{MT}) + [\text{MT}]) + k_{\text{basal}}$. **(c)** as in **a**, but in the presence of 5 μM MTs. Each point represents mean \pm SD of three individual measurements. R^2 for fits to the MD-WT and MD- Δ CT data, respectively, are **a**, 0.967 and 0.965; **b**, 0.989 and 0.988; and **c**, 0.964 and 0.945. See Supplementary Table 1 and Supplemental Information for discussion.



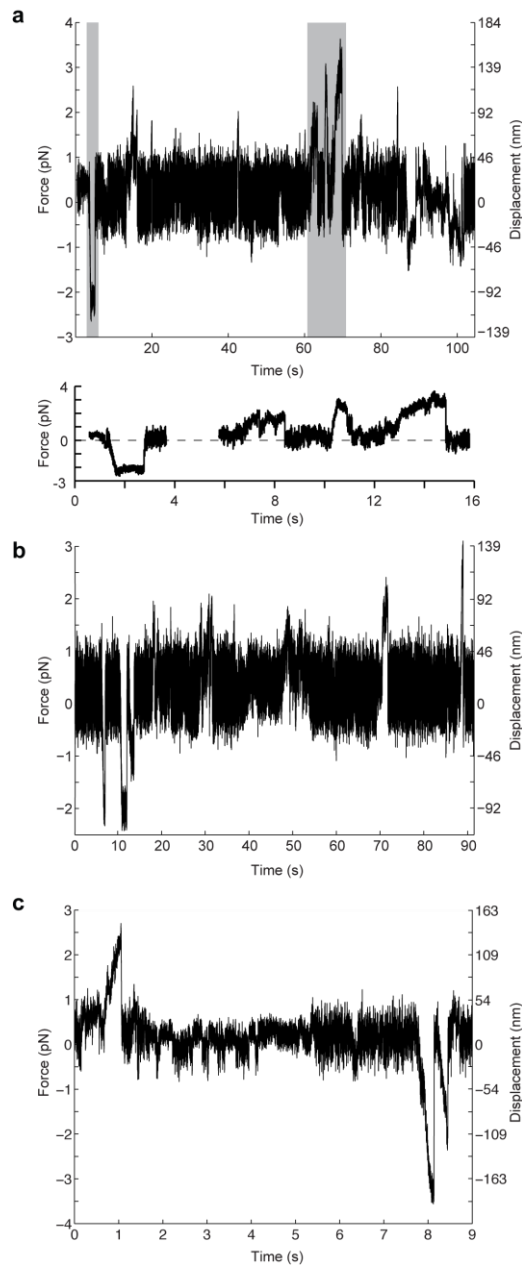
Supplementary Figure 3 | MT-gliding activity of rat dynein. Coverslips were coated with purified rat brain dynein or with anti-GST antibody, followed by MD-WT recombinant rat dynein. Results in this multi-motor assay varied by preparation and whether the protein was subjected to additional purification via size-exclusion chromatography (SEC). Lines are hyperbolic (Michaelis-Menten) fits ($v = v_{\max} \times [\text{ATP}] / (K_M(\text{ATP}) + [\text{ATP}])$) yielding maximum velocities v_{\max} and Michaelis-Menten constants $K_M(\text{ATP})$. Black circles: rat brain native dynein ($v_{\max} = 718 \pm 7$ nm/s, $K_M(\text{ATP}) = 107 \pm 4$ μM , $R^2 = 0.999$). Red upward triangles: undiluted rat GST-dynein without SEC purification ($v_{\max} = 122 \pm 1$ nm/s, $K_M(\text{ATP}) = 8.7 \pm 0.5$ μM , $R^2 = 0.996$). Blue downward triangles and green diamonds: undiluted rat GST-dynein from separate SEC fractions containing little ($v_{\max} = 356 \pm 8$ nm/s, $K_M(\text{ATP}) = 38 \pm 4$ μM , $R^2 = 0.996$) or no ($v_{\max} = 460 \pm 11$ nm/s, $K_M(\text{ATP}) = 93 \pm 9$ μM , $R^2 = 0.995$) free GST, respectively. Error bars are \pm SEM of 50-300 velocity measurements. See also Supplemental Information and Supplementary Video 1.



Supplementary Figure 4 | Gallery of additional representative examples of MD-WT force generation at motor concentrations for which 50% or fewer beads moved. This figure provides examples in addition to those of Fig. 2C of the main text. Prolonged stalling, as exhibited in the lower two traces, was exceedingly rare (~1-2% of events). Experiments were performed with AC-purified and AC-/SEC-purified protein.

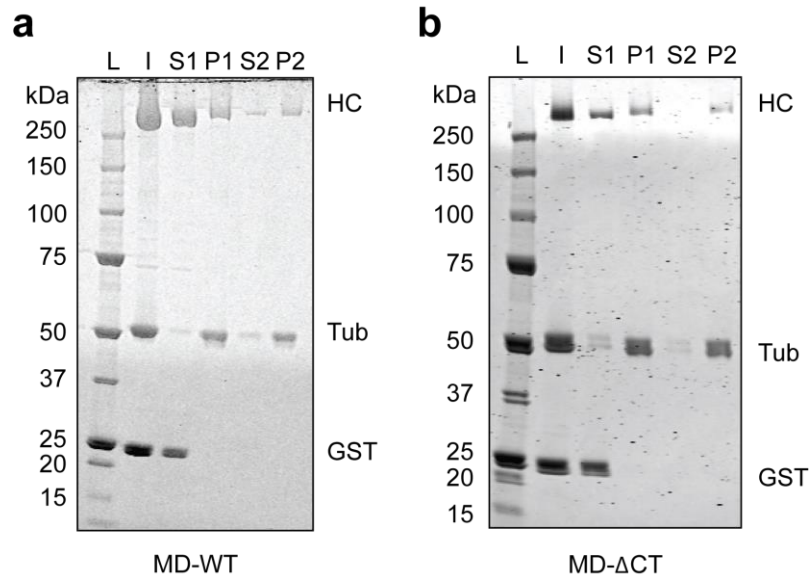


Supplementary Figure 5 | Histogram of maximal forces achieved by MD-WT during individual MT encounters. Data represent 381 events derived from 54 beads over 19 separate experiments. The spring constant used was $k = 0.01$ pN/nm. The mean and SD were calculated from the raw data without fitting. Experiments were performed with AC-purified and AC-/SEC-purified protein.

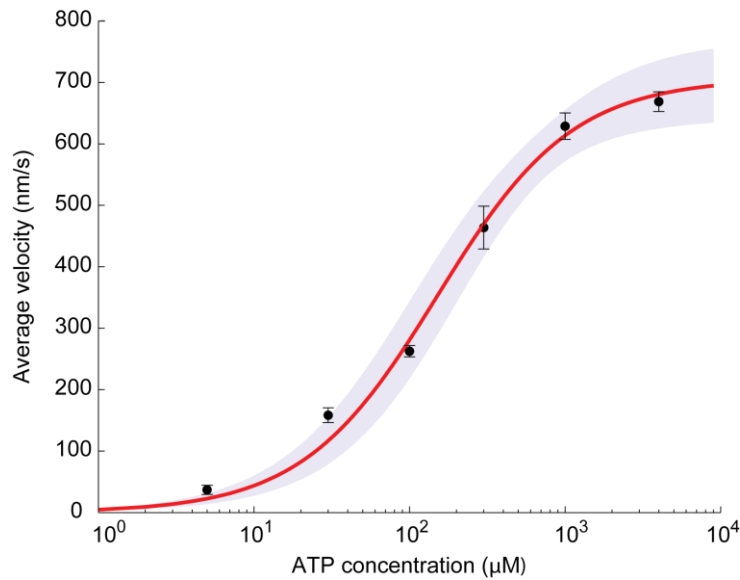


Supplementary Figure 6 | Examples of bidirectional motion at high MD-WT

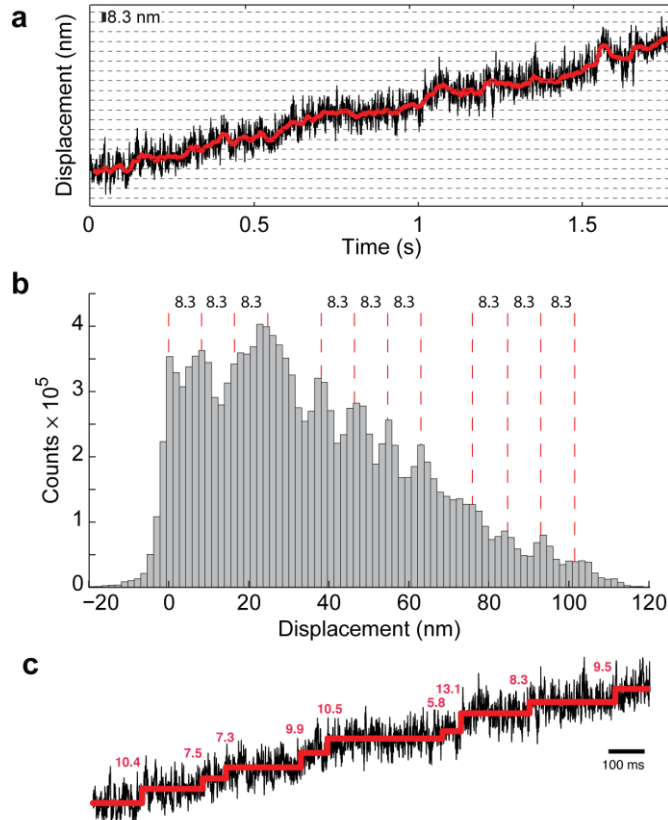
concentrations. (a-c) Example records of bidirectional force generation events at high MD-WT concentrations (several times that needed for 100% bead movement). The lower inset in **a** shows detailed views of the regions boxed in gray on the main axes. Experiments were performed with AC-purified protein.



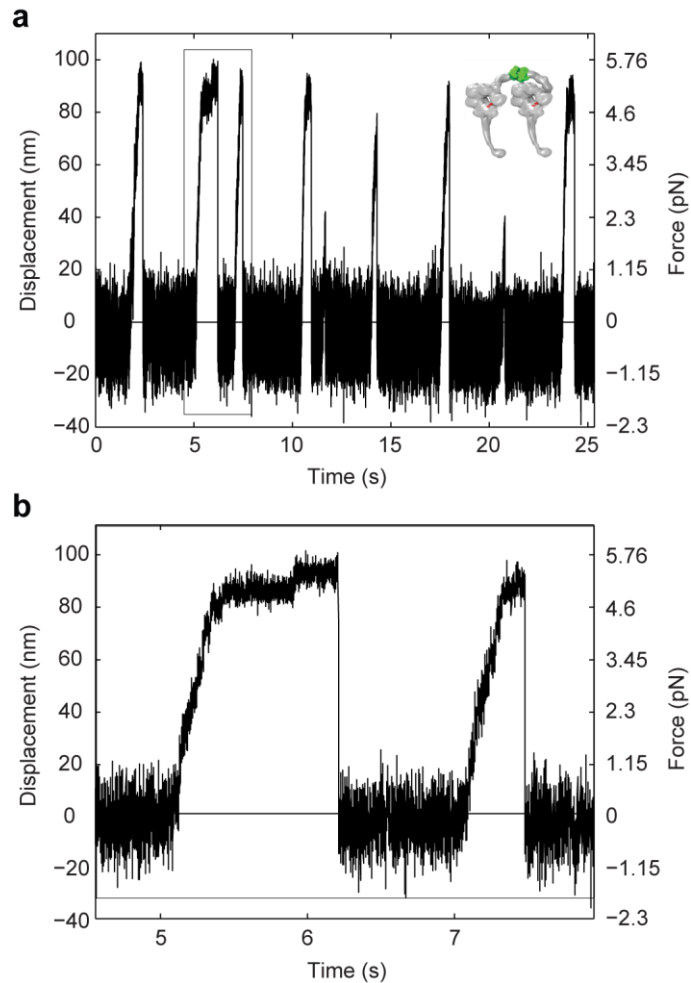
Supplementary Figure 7 | MT cosedimentation and release purification. (a) SDS-PAGE gel (Krypton stain) for MD-WT (360 ng/ μ L input). (b) as in a, but for MD- Δ CT (80 ng/ μ L input). Dynein was added to MTs (final tubulin concentrations: 2 μ M for MD-WT and 3 μ M for MD- Δ CT) and cosedimented via centrifugation (P1). After removing the supernatant (S1), the MT pellet was washed and resuspended and 5 mM ATP was added to induce motor release. The MTs were again pelleted (P2), and the supernatant (S2) was reserved. L: protein ladder, I: input, HC: dynein heavy chain, Tub: tubulin, GST: free GST. See Material and Methods and Supplemental Information for discussion.



Supplementary Figure 8 | MD- Δ CT velocity under constant 0.5 pN backward load as a function of ATP concentration. Each point represents the mean of 50-230 average velocity measurements under constant 0.5 pN backward load, for runs ≥ 50 nm in length. Error bars are 95% CIs of the mean. The red curve is a weighted fit of the Michaelis-Menten equation $v = v_{\max} \times [\text{ATP}] / ([\text{ATP}] + K_M(\text{ATP}))$ to the points, yielding $v_{\max} = 706$ nm/s and $K_M(\text{ATP}) = 151$ μM (95% CI's, with Bonferroni correction, [646, 767] nm/s and [87, 216] μM , respectively). Coefficient of determination $R^2 = 0.997$. Since the velocity-vs.-[ATP] curve is well described by a hyperbola, our data suggest that the step size is insensitive to [ATP], assuming the underlying ATP-hydrolysis rate truly follows Michaelis-Menten kinetics (any underlying cooperative ATPase kinetics with a sigmoidal [ATP]-response would result in a velocity-vs.-[ATP] curve with even higher sigmoidicity, if the step size increased from the ~ 8 nm observed at low [ATP]; Supplementary Fig. 9). Experiments were performed with AC-purified protein.



Supplementary Figure 9 | Example of MD- Δ CT stepping under 0.5 pN constant load at 5 μ M ATP. (a) Raw data (black) and data after application of a median filter with 30 ms window (red). No steps larger than \sim 8 nm are resolvable by eye (trap stiffness: $k = 0.031$ pN/nm). **(b)** Pairwise distance distribution function (PDF) calculated from the filtered data in **a**. Groups of gridlines (red) demonstrate the predominance of \sim 8.3-nm separations between apparent peaks (shifting of peaks from exact 8.3 nm multiples and apparent missing peaks are likely due to instrument positional drift). **(c)** Step-size analysis of the raw data in **a** (0-1.5 s trace segment) using the step-finding algorithm developed by Kerssemakers et al. (4). The raw data are shown in black and the steps detected by the step-finding program in red. The analysis agrees with the predominance of \sim 8 nm steps as revealed by the PDF in **b**. Experiments were performed with AC-purified protein.



Supplementary Figure 10 | Example record of force generation by MD- Δ CT at high motor concentration. (a) Force/motion trace showing repeated force generation events in the trap up to ~ 5.5 pN (trap stiffness: $k = 0.058$ pN/nm) at a motor concentration at which all trapping beads tested ($N = 16$) either bound only or moved along MTs. (b) Trace segment corresponding to the trace section indicated by the rectangular box in **a** showing a motor stalling event. As the motor approaches stalling, the velocity slows considerably, and ~ 8 -nm steps are clearly resolvable. Experiments were performed with AC-purified protein.

Supplementary Tables:

	Basal ATPase (No MTs)		MT-Stimulated ATPase				
	k_{cat} (s ⁻¹)	$K_M(\text{ATP})$ (μM)	k_{basal} (s ⁻¹)	k_{cat}' (s ⁻¹)	$K_M(\text{MT})$ (μM)	k_{cat}'' (s ⁻¹)	$K_M(\text{ATP})'$ (μM)
MD-WT	6.8 ± 0.1	172 ± 16	7.6 ± 0.5	17.3 ± 0.7	1.60 ± 0.46	13.3 ± 0.7	114 ± 24
MD-ΔCT	11 ± 2	6,800 ± 2,000	0.31 ± 0.4	9.7 ± 0.6	1.34 ± 0.36	8.2 ± 0.9	587 ± 200

Supplementary Table 1 | Summary of ATPase activity (per dimer). Values are given from the fits in Supplementary Fig. 2, ± standard errors of the fit values. k_{cat} is the maximal ATPase rate in the absence of MTs and $K_M(\text{ATP})$ is the ATP concentration producing a rate of $\frac{1}{2}k_{cat}$ in the absence of MTs (see Supplementary Fig. 2A). k_{basal} , k_{cat}' , and $K_M(\text{MT})$ were all measured in the presence of 1 mM ATP (see Supplementary Fig. 2B). Thus, k_{basal} is the ATPase rate in the absence of MTs for this particular ATP concentration; k_{cat}' maximally MT-stimulated rate at 1 mM ATP, and $K_M(\text{MT})$ is the MT concentration yielding $\frac{1}{2}k_{cat}'$. k_{cat}'' and $K_M(\text{ATP})'$ are analogous to k_{cat} and $K_M(\text{ATP})$, respectively, except that 5 μM MTs were present (see Supplementary Fig. 2C). See Supplemental Information for discussion.

$K_M(\text{ATP})$ (μM)	Species	MT conc. (μM)	Reference
15	Cow	18	Shpetner et al. (5)
33 or 280*	Cow	NA (MT gliding)	Shimizu et al. (6)
89	Pig	NA (optical trapping)	Toba et al. (7)
27	Mouse	10	Ori-McKenney et al (8)
18	<i>D. discoideum</i>	10	Kon et al. (9)
26	<i>S. Cerevisiae</i>	5	Cho et al. (1)

Supplementary Table 2: Reported $K_M(\text{ATP})$ values for cytoplasmic dynein. NA: not applicable. *Different methods of calculation yielded different results.

Supplementary Note:

Notes on bidirectional motility observed at high motor concentration

Bidirectional motion was observed only at very high motor concentrations (100% of beads exhibiting motion), and never at the single-molecule level ($\leq 50\%$ beads exhibiting motion). The behavior occurred on multiple MTs and also on axonemes. However, it was not observed for every bead tested under these conditions, and backward movement was often seen only sporadically. This may indicate that reversal of movement only occurs for specific configurations of grouped motors. Kinesin contamination was highly unlikely given the expression and purification strategies, as well as the specific linkage of the motor to the bead via an anti-GST antibody. Careful visual inspection of the fluorescence-labeled MTs that supported bidirectional motion never revealed any evidence of MT bundling that might lead to antiparallel tracks for the motors to move upon.

Bidirectional movement was only observed once for MD- Δ CT (again, at very high motor concentration). This may reflect an inherent difference between MD-WT and MD- Δ CT.

However, we believe it is more likely explained by the relatively low fraction of active MD- Δ CT motors in our preparations (see below), which would decrease the likelihood of active motors attaching near each other on the trapping bead surface. Consistent with this, even at relatively high motor concentrations, the behavior of MD- Δ CT (e.g. velocity and stall force) was not noticeably changed from that at the single-molecule level, suggesting that even at high concentrations, single motors drove the vast majority of events (Supplementary Fig. 10).

Notes on the proportions of active dynein motors

Our purified MD-WT and MD- Δ CT samples were well behaved as judged by the absence of degradation and aggregation (Supplementary Fig. 1). However, multiple observations suggest that the MD- Δ CT construct is particularly vulnerable to loss of activity. The enzymatic rate k_{cat} obtained from ATPase assays at saturating MT concentration was variable from one preparation to the next, ranging from ~ 13 ATP/s to ~ 17 ATP/s for MD-WT and ~ 1 ATP/s to ~ 9 ATP/s for MD- Δ CT (the lower ATPase activities of MD- Δ CT might in part reflect the very high basal and MT-activated $K_M(\text{ATP})$ values for this construct determined enzymatically, see Supplementary Table 1). Low measured ATPase activity correlated with a low fraction of motile beads in the optical trapping assay (even at high motor concentrations) and some preparations of both constructs failed to produce any motility. This was probably due to inactive motors occupying the majority of the binding sites on most beads. However, the contribution of preparative conditions, freeze/thaw, and freshness to protein stability remains incompletely resolved.

Unlike MD-WT (Supplementary Fig. 3 and Supplementary Video 1), MD- Δ CT did not support MT gliding, and instead MTs bound rigidly to the motor-coated surface (Supplementary Video 2), even when diluted 10,000 \times from starting concentration. Similarly, when attempting further purification via cosedimentation with MTs followed by ATP-induced release, no detectable MD- Δ CT released from MTs, even in the presence of 5 mM ATP (Supplementary Fig. 7B). These findings might suggest that MD- Δ CT is immotile, has a slow enzymatic rate, or has a very high affinity for MTs (even in the presence of 5 mM ATP and 200 mM KCl; this behavior is partly consistent with that of yeast MD dimers, which can be extracted with inclusion of high salt, though this still had no apparent effect on rat MD- Δ CT extraction). However, the robust motility observed in the trap suggests that single MD- Δ CT motors are highly active. Indeed, we measured

the maximal velocity for the motor under low load to be ~ 700 nm/s (Fig. 3E and Supplementary Fig. 8). Given the 8-nm step size, this implies $k_{\text{cat}} \approx 90 \text{ s}^{-1}$, which is at least 10-fold greater than the result calculated from MT-stimulated ATPase measurements. This could mean that less than 10% of the motors in such a sample are active depending on the preparation. It is also notable that, under identical experimental conditions, a GST-dimerized yeast dynein analogous to MD- Δ CT supported robust MT gliding (Supplementary Video 3). Our optical trapping analysis of MT interactions of motor-coated beads further supports the conclusion that a large percentage of the MD- Δ CT motors is inactive. While trapping beads without bound motors did not show any MT interactions, beads incubated with motors either generated force and displacements or bound to MTs without detectable force-generation events. In contrast to beads coated with MD-WT motors, of which 90-100% of all MT-interacting beads generated forces above the detection limit of 0.2 pN, less than 20% of the MT-interacting beads coated with MD- Δ CT motors showed force-generation (the remaining MT-interacting beads coated with MD- Δ CT motors bound strongly to MTs without detectable force generation). To ensure single-molecule MT-interactions of either inactive or active motor molecules, these analyses were performed at motor concentrations where less than 30% of all beads tested interacted with MTs. This further supports the idea that a large fraction of inactive motors, rather than poor enzyme activity, is responsible for the results from the ensemble (ATPase and MT gliding) assays.

Given these challenges, we opted to avoid detailed mechanochemical interpretation of ensemble assays for MD-WT and MD- Δ CT, and we instead focused on unambiguous single-molecule measurements using the optical trap. It is notable that both MD-WT and MD- Δ CT retained activity in this assay up to multiple hours, suggesting that the observed loss of activity may result

from failure to properly fold during expression, damage experienced during subsequent purification steps, or denaturation during freezing/thawing of stored aliquots. This may also reflect improved enzyme stability when attached to the trapping beads. Alternatively, it is conceivable that individual motors transition between active and inactive states, spending most of their time in the latter.

Discussion of mechanisms for regulation of dynein force and processivity by the CT-cap

Considerable future work will be needed to define the precise mechanism by which removal of the CT-cap from the mammalian dynein motor domain (MD) imparts it with yeast dynein-like force production and processivity. As mentioned in the main text, one possibility is that the CT-cap controls nucleotide affinity of the AAA1 active site via direct interactions. This way the CT-cap could control force-bearing states of the dynein cross-bridge cycle and make the motor less able to withstand opposing load and more likely to release after a few steps. Some of our ATPase and MT-gliding assay results suggested a larger $K_M(\text{ATP})$ for MD- ΔCT than for MD-WT, which could indicate a difference in nucleotide affinity. However, both ensemble techniques yielded variable results depending on the protein preparation assayed. In the MT-gliding assay, in addition to variations among different preparations, the measured kinetics differed within individual preparations depending on which fraction from size exclusion chromatography was used (Supplementary Fig. 3), possibly due to assay-specific effects arising from different amounts of GST competing with the GST-tagged dynein for surface-bound anti-GST antibodies on the glass.

Single-molecule function was reproducible and far easier to interpret. MD-WT showed indistinguishable behavior on the single-molecule level whether GST fragments were present or not. Due to its limited processivity and low stall force, characterization of MD-WT $K_M(\text{ATP})$ at low load was infeasible. However, we were able to characterize the $K_M(\text{ATP})$ for MD- ΔCT (Supplementary Fig. 8) at low load (0.5 pN), yielding $K_M(\text{ATP}) = 151 \mu\text{M}$ (95% CI [87, 216] μM). Comparing this $K_M(\text{ATP})$ to values reported previously (as well as values obtained in the gliding assay for both GST-dimerized and native dynein) does not suggest a substantial difference from higher eukaryotic wild-type dyneins (although the reported values span a fairly large range) (Supplementary Table 2). Moreover, the $K_M(\text{ATP})$ reported for yeast dynein (1) (Supplementary Table 2) is nearly as small as the lowest reported values for higher eukaryotes, suggesting that removal of the CT-cap does not, by itself, drastically affect $K_M(\text{ATP})$. Nonetheless, the dramatic decrease in vanadate sensitivity caused by removal of the CT-cap (2) suggests that some step in the catalytic cycle is under the control of dynein's C-terminal domain. In conclusion, future work is needed to determine whether the CT-cap alters AAA1 function directly or acts as a “mechanical” element that affects the allosteric communication between the AAA ring and the MTBD.

Supplementary References

1. C. Cho, S. L. Reck-Peterson, R. D. Vale, Regulatory ATPase sites of cytoplasmic dynein affect processivity and force generation. *J. Biol. Chem.* **283**, 25839-25845 (2008).
2. P. Höök, A. Mikami, B. Shafer, B. T. Chait, S. S. Rosenfeld, R. B. Vallee, Long range allosteric control of cytoplasmic dynein ATPase activity by the stalk and C-terminal domains. *J. Biol. Chem.* **280**, 33045-33054 (2005).
3. M. Nishiura, T. Kon, K. Shiroguchi, R. Ohkura, T. Shima, Y. Y. Toyoshima, K. Sutoh, A single-headed recombinant fragment of Dictyostelium cytoplasmic dynein can drive the robust sliding of microtubules. *J. Biol. Chem.* **279**, 22799-22802 (2004).
4. J. W. J. Kerssemakers, E. L. Munteanu, L. Laan, T. L. Noetzel, M. E. Janson, M. Dogterom, Assembly dynamics of microtubules at molecular resolution. *Nature* **442**, 709-712 (2006).
5. H. S. Shpetner, B. M. Paschal, R. B. Vallee, Characterization of the microtubule-activated ATPase of brain cytoplasmic dynein (MAP 1C). *J. Cell Biol.* **107**, 1001-1009 (1988).
6. T. Shimizu, Y. Y. Toyoshima, M. Edamatsu, R. D. Vale, Comparison of the motile and enzymatic properties of two microtubule minus-end-directed motors, ncd and cytoplasmic dynein. *Biochemistry* **34**, 1575-1582 (1995).
7. S. Toba, T. M. Watanabe, L. Yamaguchi-Okimoto, Y. Y. Toyoshima, H. Higuchi, Overlapping hand-over-hand mechanism of single molecular motility of cytoplasmic dynein. *Proc Natl Acad Sci U S A* **103**, 5741-5745 (2006).
8. K. M. Ori-McKenney, J. Xu, S. P. Gross, R. B. Vallee, A cytoplasmic dynein tail mutation impairs motor processivity. *Nat Cell Biol* **12**, 1228-1234 (2010).
9. T. Kon, M. Nishiura, R. Ohkura, Y. Y. Toyoshima, K. Sutoh, Distinct functions of nucleotide-binding/hydrolysis sites in the four AAA modules of cytoplasmic dynein. *Biochemistry* **43**, 11266-11274 (2004).